machines

Article

Study of Diamond Wheel Wear Based on the Principle of Frictional Energy Distribution in Ultrasonic-Assisted Grinding Trajectories

Longfei Zhao [1], Sisi Li [1,2,*], Xianglei Zhang [1], Hongming Zhou [1] and Qiang Wang [3]

[1] College of Mechanical and Electrical Engineering, Wenzhou University, Wenzhou 325035, China
[2] Rui'an Graduate College, Wenzhou University, Wenzhou 325206, China
[3] Department of Mechanical and Energy Engineering, Southern University of Science and Technology, Shenzhen 518055, China
[*] Correspondence: 20200574@wzu.edu.cn

Abstract: In the grinding process, the friction energy generated by grains and the workpiece in the grinding zone will affect the service life of the grinding wheel. Ultrasonic-vibration-assisted grinding (UVAG) can reduce the friction force and reduce the generation of friction energy during grinding. In this work, the wear mechanism of grinding wheels in UVAG is discussed in detail from the perspective of the grain grinding trajectory and tribology. The results show that UVAG has a smaller friction force than conventional grinding (CG). Furthermore, when the initial included angles of grains are 90° and 150°, the friction energy of a single grinding surface in UVAG is reduced by 24% and 37% compared with that of CG, respectively. In UVAG, the grains are prone to microfractures, and the self-sharpening ability of the grinding wheel is enhanced, which can obtain a lower grinding force and better grinding surface quality.

Keywords: ultrasonic-vibration-assisted grinding; wear; grinding trajectories; friction energy

1. Introduction

Zirconia ceramics are widely used in aerospace, mechanical engineering, new energy, automotive, electronics and biomedical fields due to their high-temperature resistance, wear resistance, high hardness, high strength and chemical stability [1–4]. However, it is fragile and difficult to machine, which requires expensive equipment for machine processing [5]. Cutting/milling, polishing and grinding are the traditional processing methods for zirconia [6,7]. In order to solve challenges in obtaining high-accuracy products, grinding is the main method for machining ceramic components. The grinding process is an effective processing method that uses a diamond grinding wheel with higher hardness that can grind zirconia materials with hard and brittle characteristics [8]. In conventional grinding (CG), tools will inevitably produce high grinding forces and grinding temperatures, resulting in wear [9].

To address the problem of CG, a variety of assisted grinding technologies came into being, such as laser-assisted grinding, electric discharge grinding and ultrasonic-assisted grinding [10–12]. Laser-assisted grinding is a method that uses a focused laser beam to locally heat and soften workpiece materials. This method reduces the grinding energy and improves the material removal rate and surface quality [13,14]. However, the thermal damage and heat-affected zone caused by the laser will remain on the surface of the workpiece, adding processing steps. Electric discharge grinding is a method of softening material by high-temperature discharge, which reduces the grinding force and increases the material removal rate [15,16]. This method is only applicable to metal-bonded grinding wheels. Due to the conductive effect of the metal binder, the loss of the binder and the wear of the grinding wheel will be accelerated [17]. UVAG is a processing technology that

combines ultrasonic vibration and grinding. Ultrasonic vibration is applied to the tool, changing its kinematics [18]. This method combines the material removal mechanism of grinding and the characteristics of ultrasonic vibration, which reduces the grinding force, thermal damage, friction and wear in the grinding process. In contrast, ultrasonic-assisted grinding has more advantages. It is an advanced processing technology suitable for hard and brittle materials. Therefore, many scholars have conducted extensive research on the grinding wheel wear mechanism during ultrasonic-assisted grinding.

Kai Ding [19] studied the wheel wear behavior when grinding silicon carbide ceramics. The results showed that grain fracture was the main wear form of UVAG, while attrition wear was the main wear mode during CG. At the same time, the UVAG grinding force was lower and more stable than CG. In other research, J.Y. Shen [20] used diamond grinding wheels to grind alumina ceramics. The results showed that UVAG was beneficial to the microfracture of grains, and the number of active cutting edges in UVAG is more than that in CG, which improved the self-sharpening of grinding wheels. However, the mechanism of grain microfracture in UVAG was not explained. Mohammad Baraheni [21] studied the grinding force model of silicon carbide ceramics in UVAG and pointed out that the increase in the semi-angle of the grains means grain wear, which leads to an increase in the grinding force. Xiaofei Lei [22] carried out UVAG grain wear experiments, and the results showed that the grinding force increased with the increase in grain wear. Zhiqiang Liang [23] pointed out that the UVAG grinding wheel has a longer sharp-cutting period than the CG grinding wheel due to the microfracture of UVAG grains in sapphire grinding experiments. In addition, the friction effect in UVAG will affect the wear form of the grinding wheel, but the mechanism of ultrasonic friction reduction was not discussed in detail.

At present, most studies focus on the form of UVAG grinding wheel wear, but the relationship between wheel wear and frictional energy has not been determined, which is significant for controlling wheel wear. The friction energy generated by the grains and the workpiece in the grinding zone will affect the service life of the grinding wheel. To further study the relation between the friction energy distribution and grain wear in UVAG, a diamond grinding wheel was used to grind zirconia ceramics in CG and UVAG. The surface morphology of the grinding wheel was observed by SEM (scanning electron microscopy) and laser confocal microscopy, as was the grain morphology before and after grinding. The wear behavior of the grinding wheel that changed with processing parameters in CG and UVAG was explored in detail, and the wear mechanism of the grinding wheel in UVAG was analyzed from the perspective of the grinding trajectory and friction energy distribution of the grinding surface. In addition, the influence of grinding wheel wear on the grinding force and surface quality was analyzed.

2. Processing Principle and Experimental Device

2.1. Processing Principle

The axial ultrasonic-assisted grinding model is shown in Figure 1. The grinding wheel with the diameter d_s rotates anticlockwise around its own axis at the grinding speed v_s and ultrasonically vibrates on its own axis, while the workpiece is fed in the *x*-negative direction at the feed speed v_w. The motion of the grinding wheel grain is synthesized from the following three kinds of motion: rotational motion around the axis of the grinding wheel, horizontal movement relative to the workpiece and ultrasonic vibration along the axial direction of the grinding wheel. Figure 1a shows that the trajectory of the grain under CG is a straight line, and the trajectory of the grain under UVAG is a periodically varying sinusoidal function. Setting the point of entry of the grain in grinding as the coordinate origin and establishing the coordinate system shown in Figure 1b, the equation of the trajectory of the grain can be expressed as Equation (1):

$$\begin{cases} x(t) = v_w t + r\sin(\omega_s t) \\ z(t) = A\sin(\omega t) \\ y(t) = r(1 - \cos(\omega_s t)) \end{cases} \tag{1}$$
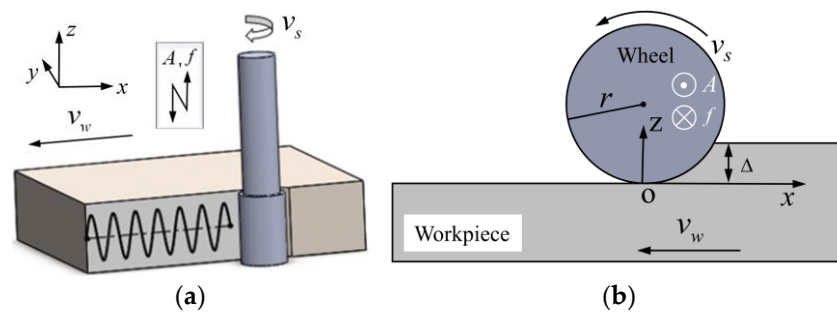
Figure 1. UVAG processing: (**a**) processing principle and (**b**) kinematics of grinding wheel.

The velocity of the grain can be obtained from the equation of the trajectory of the grain, as follows:

$$\begin{cases} v_x = v_w + r\omega_s \cos(\omega_s t) \\ v_z = A\omega \cos(\omega t) \\ v_y = r\omega_s \sin(\omega_s t) \end{cases} \tag{2}$$

where ω is the angular frequency of ultrasonic vibration and its value is $2\pi f$; ω_s is the angular velocity of the grinding wheel; and t is the movement time of the grains.

2.2. Experimental Setup

In this experiment, an axial ultrasonic-assisted zirconia ceramic grinding experimental platform was built by installing an ultrasonic tool holder (Yue Jiang ultrasonic processing unit, UB40-C5-BT40, Tokyo, Japan) at the high-precision three-axis CNC machining center, as shown in Figure 2a. The ultrasonic tool holder was mounted on the CNC machining center with a 6 mm diameter diamond grinding wheel fixed at the front of the ultrasonic tool holder, and ultrasonic vibration was applied along its axial direction. The tool vibration frequency was 50 kHz, and the amplitude was 3.3 μm, which was measured using a laser Doppler vibrometer, as shown in Figure 2b,c. In addition, a six-component piezoelectric force gauge (Kistler Instruments cutting force measurement system, 9139A, Switzerland) and a work stand were installed between the ultrasonic tool holder and the table to fix a zirconia ceramic sample with dimensions of L20.5 × W20 × T5.6 mm as a workpiece on the CNC machine table.

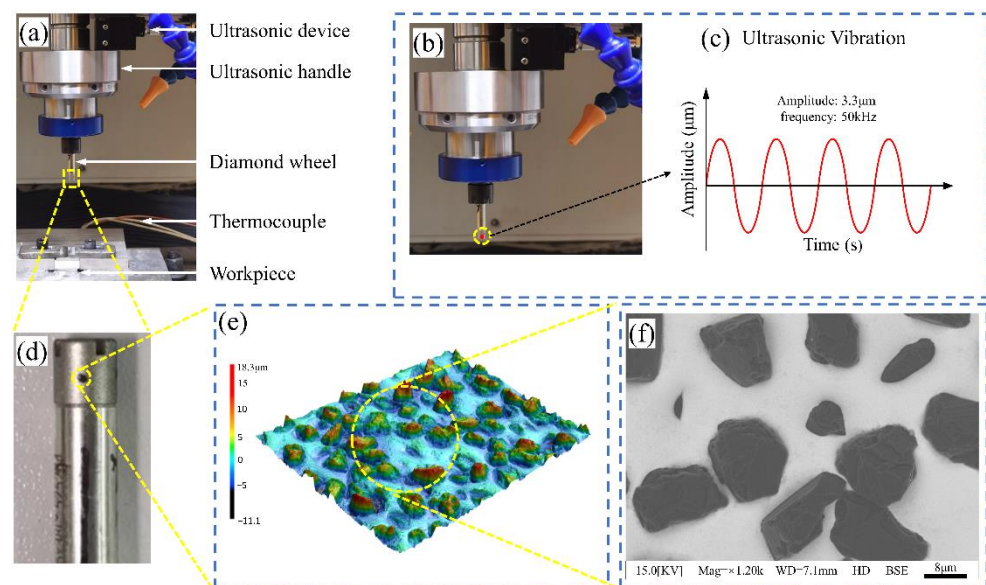**Figure 2.** Grinding experimental setup: (**a**) experimental platform, (**b**) vibration meter, (**c**) display, (**d**) abrasive wheel, (**e**) three-dimensional morphology of grains, (**f**) surface morphology of grains.

2.3. Experimental Conditions and Process

As shown in Figure 2e,f, SEM and laser confocal microscopy were used to obtain the surface morphology and three-dimensional morphology information of the grinding wheel grains, which was used to study the wear characteristics of grinding wheel wear with changes in machining parameters in CG and UVAG. For determining grain wear, the working surfaces of the employed wheel were measured, and fifty grains were measured. The experiments were conducted using single-factor experiments to study the grain wear, grinding force and surface quality of the workpiece after grinding with changing machining parameters. The specific grinding processing conditions are shown in Table 1.

Table 1. Grinding parameters.

Contents	Values
Grinding type	Flat surface grinding
Abrasive wheel	Diamond wheel (6D*6A*R0.5*38 L)
Ultrasonic frequency f	50 kHz
Ultrasonic amplitude A	3.3 μm
Grinding speed v_s	4000, 5000, 6000, 7000, 8000 (rpm)
Workpiece speed v_w	100, 200, 300, 400, 500, 600 (mm/min)
Depth of cut Δ	10, 15, 20, 25, 30 (μm)

3. Experimental Results

3.1. Grinding Wheel Wear

As shown in Figure 3, the wear of diamond grains was observed by tracking the grains before and after grinding zirconia ceramics, and the wear types were microfractures, macrofractures, drop-outs and adhesion wear.
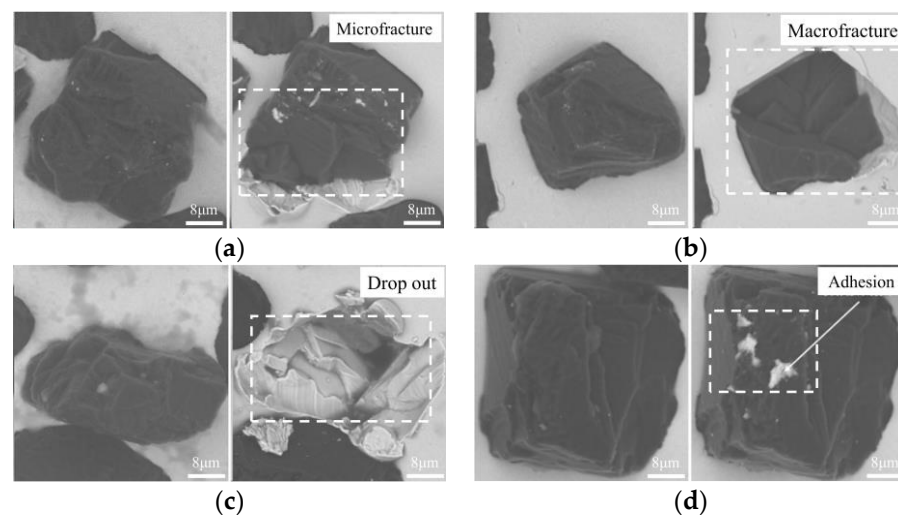

Figure 3. Grain wear: (**a**) microfracture, (**b**) macrofracture, (**c**) drop-out and (**d**) adhesion.

Figure 4 shows the different wear types of the grains in CG and UVAG. The grinding direction of the grains in CG is unchanged, and only a single fracture surface is generated along the grinding direction. Different grains will form different fracture shapes, as shown in Figure 4a,b. In UVAG, the grinding direction of the grains changes, and the grains produce multiple fracture surfaces along the grinding direction, resulting in more cutting edges. The fracture sizes of different grains vary, as shown in Figure 4c,d. Therefore, the self-sharpening ability of the grains in UVAG is stronger. The reasons for the multiple fracture surfaces of grains in UVAG will be discussed and analyzed in the following.
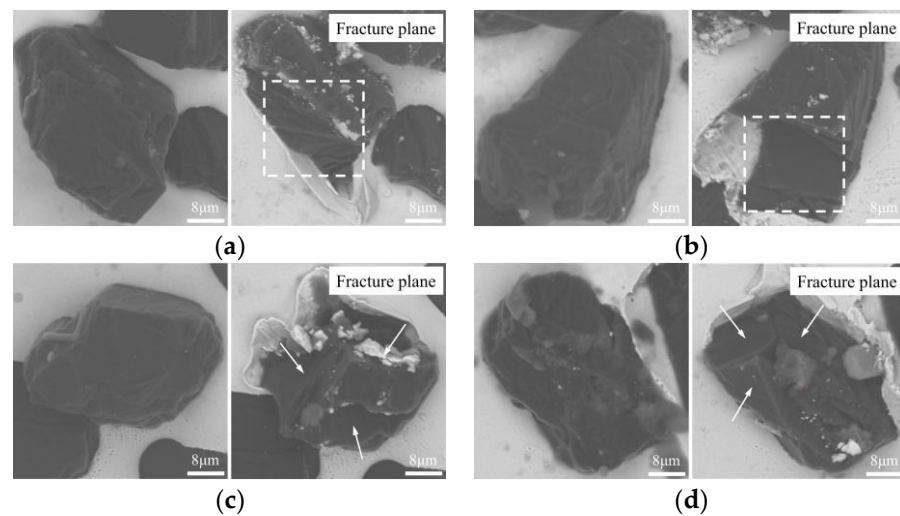
Figure 4. Wear of grains: (**a**,**b**) normal grinding and (**c**,**d**) ultrasonic-assisted grinding.

The worn grains in CG and UVAG were counted, as shown in Figure 5. With increasing spindle speed, the drop-out and microfracture of the grains decreased in both CG and UAG, as shown in Figure 5a. Compared with CG, the number of drop-outs in UVAG decreased by 54.3%, and the number of microfractures increased by 73%. With the increase in feed speed and grinding depth, the number of drop-outs and microfractures in both grinding methods increased. With the increase in feed speed, the number of UVAG grain drop-outs decreased by 44% compared with CG, and the number of grain microfractures increased by 75%, as shown in Figure 5b. With the increase in grinding depth, the number of UVAG grain drop-outs decreased by 24.5% compared with CG, and the number of grain microfractures increased by 55.5%, as shown in Figure 5c. Therefore, UVAG reduces the number of grain drop-outs and improves the grain microfracture rate.
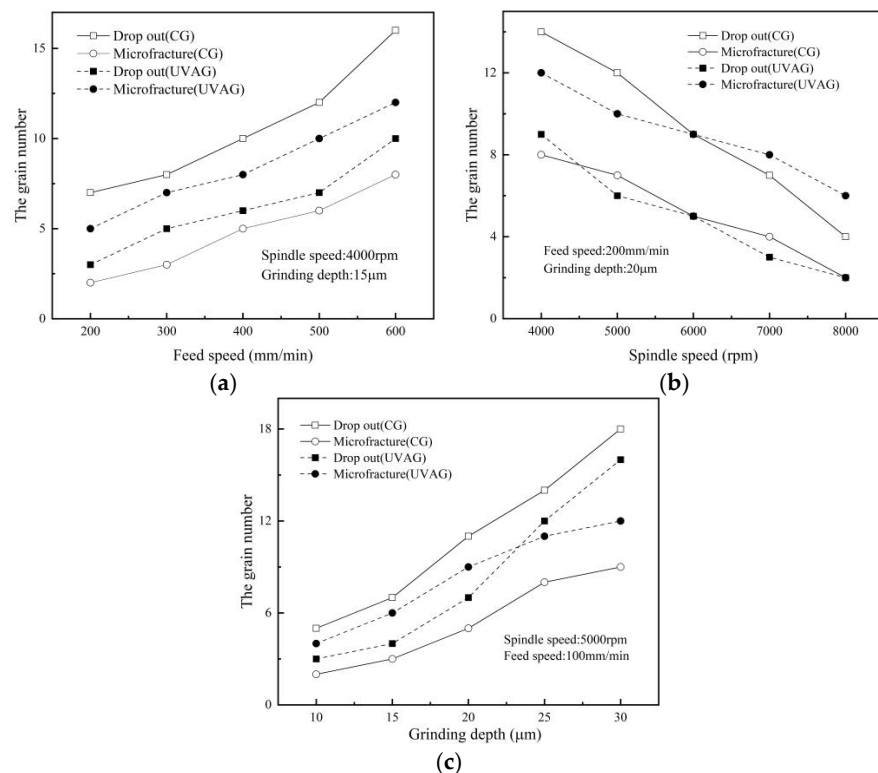

Figure 5. Grain wear in CG and UVAG: (**a**) feed rate, (**b**) spindle speed and (**c**) grinding depth.

3.2. Grinding Forces

As the grinding force is a crucial factor for measuring the grinding characteristics, Figure 6 shows the grinding forces in CG and UVAG grinding. The relationship between the spindle speed and grinding force is shown in Figure 6a. Compared with CG, as the spindle speed increases from 4000 rpm to 8000 rpm, the normal grinding force of UVAG is reduced by 21%, and the tangential grinding force is reduced by 29.7%. The relationship curve between the grinding depth and grinding force is shown in Figure 6b. Compared with CG, when the grinding depth increases from 10 μm to 30 μm, the normal grinding force of UVAG is reduced by 23.1%, and the tangential grinding force is reduced by 26.8%. As shown in Figure 6c, compared with CG, when the workpiece feed rate increases from 200 mm/min to 600 mm/min, the normal grinding force of UVAG is reduced by 18%, and the tangential grinding force is reduced by 22.3%, indicating that a much greater grinding force decrease rate can be achieved by the synergistic effect of the ultrasonic vibration and grain motion compared with CG.
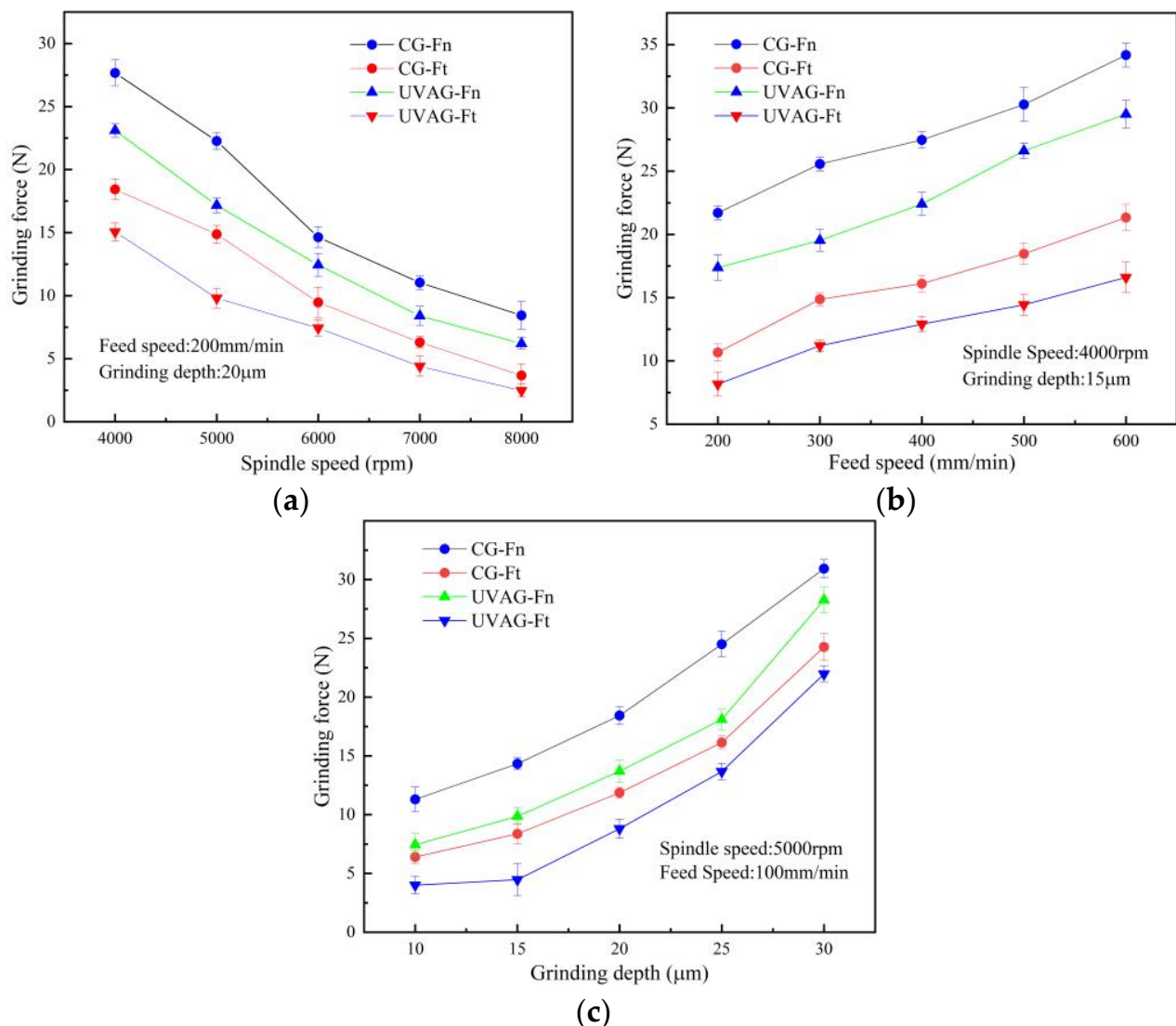

(**a**)

(**b**)

(**c**)

Figure 6. Experimental results of the grinding force: (**a**) spindle speed, (**b**) feed rate and (**c**) grinding depth.

3.3. Surface Quality

Figure 7 shows the work surface morphology and profile waves obtained with the same machining parameters in CG and UVAG. As seen in Figure 7a, the CG surface exhibits pits, cracks and scratch defects. In UVAG, no pits and cracks appear on the work surface, and only scratches are observed. Meanwhile, the CG and UVAG surface topography profile waves were extracted using software to analyze the workpiece surface characteristics, as shown in Figure 7c,d. The profile wave elements contain wave peaks and troughs, and the average height of the profile wave can be expressed as Equation (3) [24]:

$$h = \frac{1}{m}\sum_{1}^{m} h_i \tag{3}$$

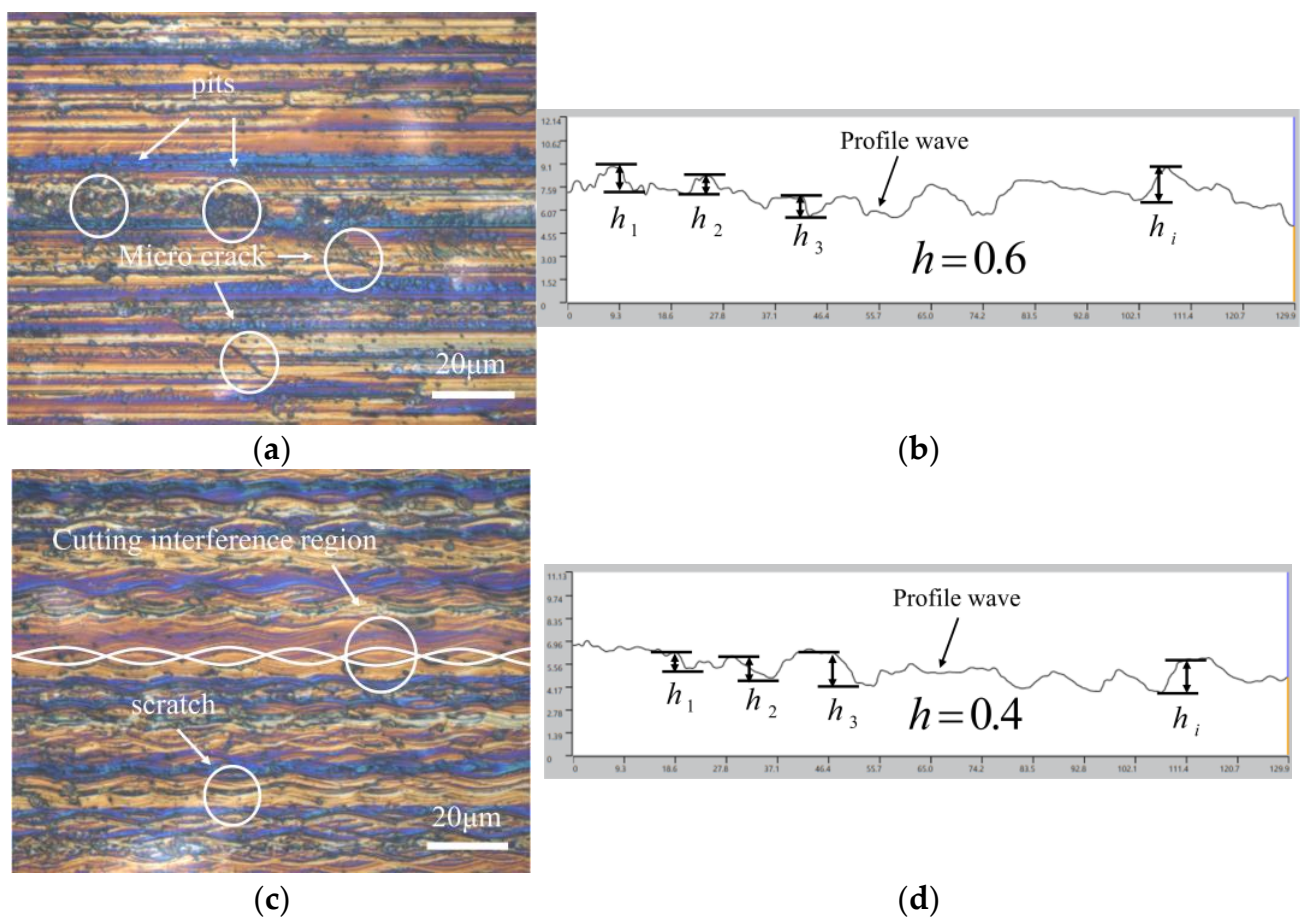where *m* is the number of measurement points, and h_i is the height of random measurement points.

(a)

(b)

(c)

(d)

Figure 7. Surface morphology and profile wave: (**a**) CG surface morphology, (**b**) CG profile wave, (**c**) UVAG surface morphology and (**d**) UVAG profile wave.

As shown in Figure 7, the average height of the UAVG profile wave is smaller. For this reason, little plastic deformation and no crater patterns were observed during grinding. Therefore, the UVAG-processed workpiece surface is smoother. Figure 8 shows that the grinding surface *Ra* value decreases with increasing spindle speed and increases with increasing feed rate and grinding depth. The wear condition of the grinding wheel is closely related to the surface quality of the workpiece, as shown in Figure 5. The improved fracture performance of the grains with UVAG leads to better surface quality.
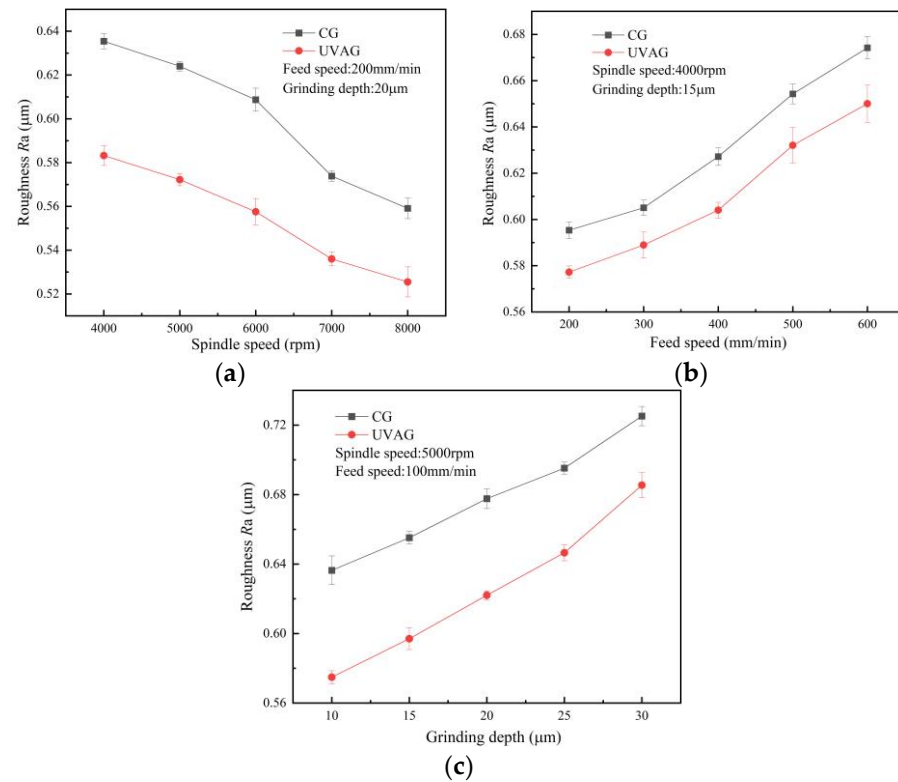
Figure 8. Roughness changes with machining parameters: (**a**) feed rate, (**b**) spindle speed and (**c**) grinding depth.

4. Discussion

4.1. Grain Wear

Ultrasonic vibration reduces the friction between the tool and the workpiece and between the tool and the chip, reducing the wear of the tool [25,26]. The ratio of the friction force $\lambda(\zeta)$ under axial ultrasonic vibration can be calculated by the following equation [27]:

$$\lambda(\zeta) = \frac{1}{2\pi} \int_0^{2\pi} \frac{\zeta + \cos\theta \cos\tau}{\sqrt{\zeta^2 + 2\zeta \cos\theta \cos\tau + \cos^2\tau}} d\tau \tag{4}$$

where ζ is the ratio of the macroscopic velocity of the workpiece to the amplitude of the vibration velocity, θ is the angle between the vibration direction and the velocity direction of the workpiece, and τ is the normalization time ($\tau = \omega t$).

The expression of the grain speed under UVAG can be obtained as:

$$v_r = \sqrt{v_x^2 + v_y^2 + v_z^2} \tag{5}$$

During one revolution of the grinding wheel, the contact time t_1 between each grain and the workpiece and the cutting length of a single grain in CG and UVAG can be expressed as Equation (6) [28]:

$$\begin{cases} t_1 = \arccos(1 - a_e/r)/2\pi n \\ l_{CG} = \int_0^{t_1} \sqrt{v_x^2 + v_y^2} dt \\ l_{UVAG} = \int_0^{t_1} \sqrt{v_x^2 + v_y^2 + v_z^2} dt \end{cases} \tag{6}$$

where a_e is the depth of cut. Due to the random distribution of grains on the grinding wheel, different grains have different initial included angles during grinding. The different initial angles will cause different grinding surfaces to participate in grinding, resulting

in different cases of wear. In CG, the grinding surface will not be changed in subsequent grinding after the grinding grain plunge angle is determined because the grinding trajectory remains unchanged. In UVAG, the grinding trajectory of grains is sinusoidal, and even though the grain defines a certain grinding surface with a certain tangent angle, the angle θ between the speed direction of the grain and the grinding direction (as shown in Figure 9b) dynamically changes. This causes the grinding surface to change during grinding, resulting in special wear.
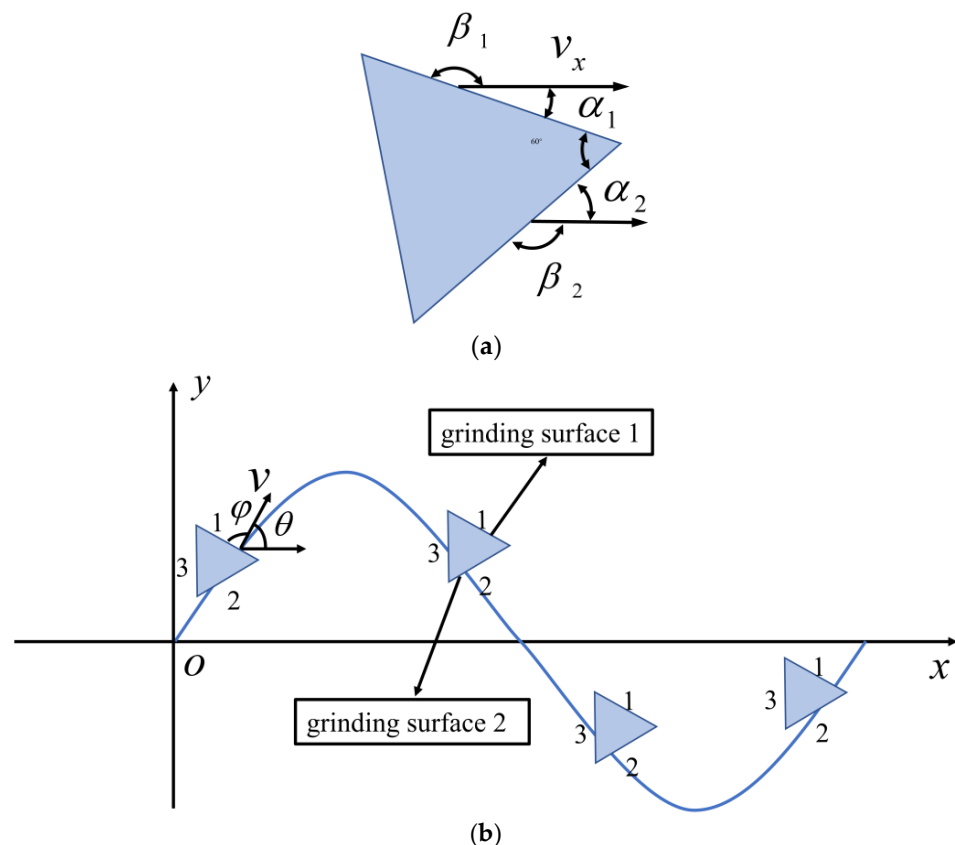

Figure 9. Analysis of single-grain grinding: (**a**) initial included angle of grains and (**b**) grain grinding path.

Because the maximum thickness of the undeformed chip in single-grain grinding is far less than the grain height, the actual grinding accounts for only part of the grains involved in the material removal process. To study the effect of UVAG grinding surface changes on wear, the grains were simplified to regular triangles, and the initial included angle of grain grinding was analyzed, as shown in Figure 9a. The angle of the grain plunge β_1 is assumed to be the angle between the grinding surface and the grinding direction, and the angle between the grain velocity direction and the grinding surface during grinding is φ. When $180° < \varphi$, the grinding surface will change, as shown in Figure 9b. According to Figure 9a, the relationship of each angle can be shown by the following equation:

$$\begin{cases} \beta_1 + \alpha_1 = 180° \\ \alpha_1 + \alpha_2 = 60° \\ \alpha_2 + \beta_2 = 180° \end{cases} \tag{7}$$

During grinding, the normal grinding force during the cutting of a single grain is shown by the following equation [29]:

$$F_N = \beta' \left(\frac{K_{IC}^{1/2} H^{9/10}}{E_w^{2/5}} \right) \left(\frac{V_w}{V_s} \right)^{3/4} a_e^{11/12} r^{1/6} \tag{8}$$

where β' is a constant related to the grinding wheel topography information, K_{IC} is the material fracture toughness, H is the material Vickers hardness, and E_w is the material elastic modulus.

The frictional energy generated by the friction force of a single grain in a rotation cycle of the grinding wheel can be expressed as the following equation:

$$\begin{cases} W_{UVAG} = \int_0^{t_1} \mu_{UVAG} F_N l_{UVAG} \sin(\alpha_1 + \frac{t}{360°f})dt \\ W_{CG} = \mu_{CG} F_N l_{CG} \sin \alpha_1 \end{cases} \tag{9}$$

The friction energy between CG and UVAG at arbitrary initial included angles of grains is shown in Equation (9). Compared with CG, it can be seen that the single grinding surface in UVAG bears lower friction energy. However, the cut in the angle of the grains is complex. To quantify the friction energy of a single grain in UVAG and CG, the two special situations are discussed and analyzed.

The friction energy generated by a single grinding surface is maximum when the grinding grain is cut into the angle $\beta_1 = 90°$. The grinding trajectory of a single grinding grain in CG and UVAG is shown in Figure 10.

(a)
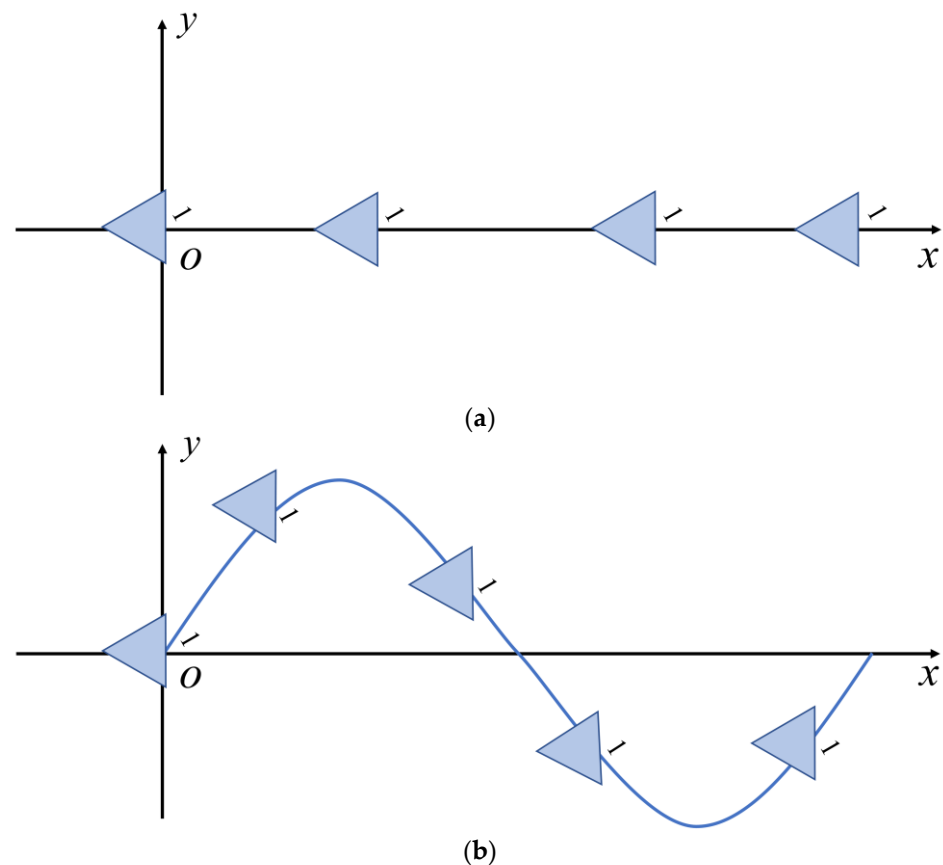

(b)

Figure 10. Grinding trajectory: (**a**) CG and (**b**) UVAG.

As shown in Figure 10a, when the initial included angle β_1 is 90°, Grinding Surface 1 in CG is always involved in grinding. Figure 10b shows that angle β_1 is always less than 180° during one grinding vibration cycle of UVAG. Then, the grinding surface does not change, and Grinding Surface 1 is always involved in UVAG. To compare the effects of the two grinding methods on Grinding Surface 1, the difference in the effect of the two grinding methods on grain wear was elucidated by using the single-grain friction work in one cycle. From Equations (6)–(9), the friction energy is reduced by 24% compared to that in CG.

When the grain's initial included angle β_1 is 150°, the friction energy is divided equally by Grinding Surface 1 and Grinding Surface 2 in CG. The single-grain grinding path in CG and UVAG is shown in Figure 11.
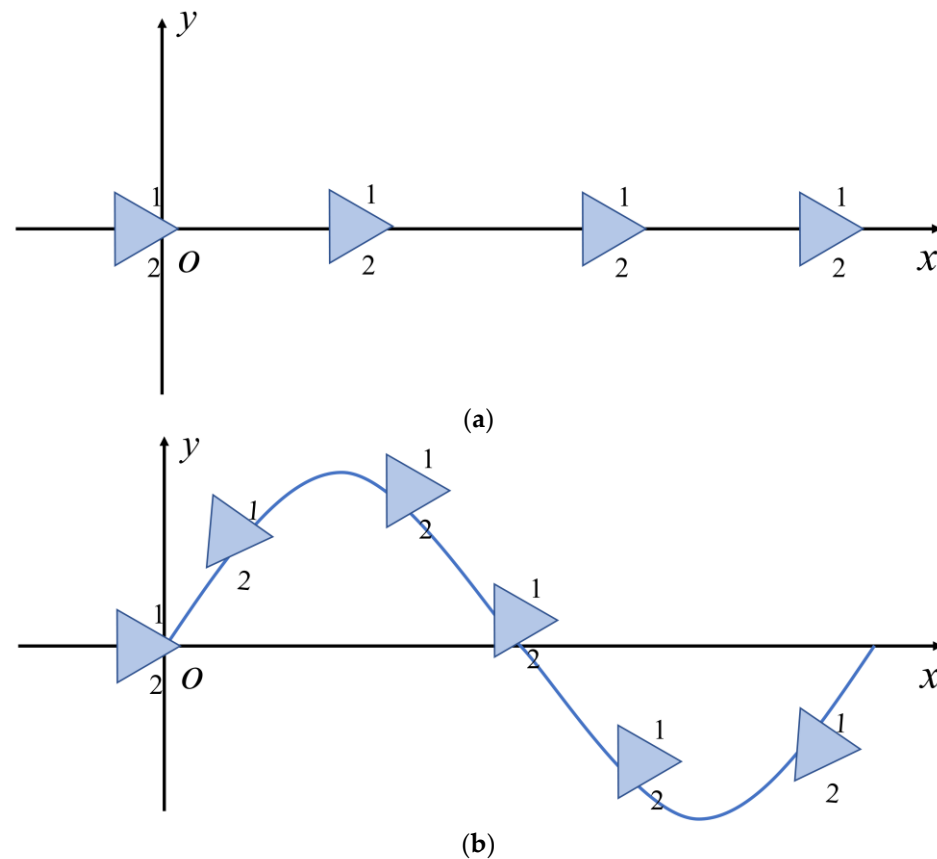

(**a**)

(**b**)

Figure 11. Grinding trajectory: (**a**) CG and (**b**) UVAG.

From Figure 11a, when the grinding grain is tangentially ground at 150°, Grinding Surface 1 and Grinding Surface 2 are always involved in the whole grinding process in CG grinding. The frictional force in CG grinding is equally shared between the two grinding surfaces, i.e., $W_1 = W_2 = 1/2\,W_{CG}$. In UVAG, the grinding speed intersects with Grinding Surface 1 at the start of grinding, and Grinding Surface 1 is involved in grinding, as shown in Figure 11b. As the grinding speed direction keeps changing, when the grinding speed direction is parallel to Grinding Surface 1, the grinding surface is transformed; i.e., Grinding Surface 2 is involved in grinding. Unlike CG, the friction force in UVAG acts on one grinding surface, but the action time is shorter than CG. As seen in Figure 11b, 0 ~ T/4 and 3 T/4 ~T Grinding Surface 1 participate in grinding, and T/4 ~ 3 T/4 Grinding Surface 2 participate in grinding. The time for the action of Grinding Surface 1 and Grinding Surface 2 in one vibration cycle is $t_1 = t_2 = T/2$; i.e., we have $W_1 = W_2 = 1/2\,W_{UVAG}$. From Equations (6)–(9), the friction energy generated by a single grinding surface in UVAG is 37% less than that in CG.

The decrease in friction energy in UVAG leads to the difficulty of chip accumulation during chip formation. The cutting force of abrasive grains is not easy to increase continuously, and the impact process in the direction of grinding rotation is more likely to occur. When an accidental force is relatively large, grains produce microfractures. In CG, chip accumulation leads to a continuous increase in the force on the grains, resulting in macrofractures and drop-outs.

Therefore, the total frictional energy in UVAG is apportioned over multiple grinding surfaces. The resulting grain wear is mainly in the form of microfracture, producing multiple fracture surfaces, which increases the number of cutting edges during grinding

and facilitates efficient material removal, while the frictional energy in CG always acts on the same grinding surface, which is prone to the macrofracture and drop-out of grains. In summary, compared with CG, UVAG has fewer grain drop-outs and more microfractures, which effectively improves the self-sharpening of the grinding wheel.

4.2. Grinding Force

The grinding force is one of the effective methods for monitoring the condition of the grinding wheel and assessing the grinding performance [30]. From the above analysis, the friction energy generated in UVAG is distributed to multiple grinding surfaces of grains. The friction energy of the grinding surface of a single grain is reduced, and the grains in UVAG easily undergo microfracture to produce a new cutting edge. Therefore, the self-sharpening performance of the UVAG grinding wheel is improved, and the grinding force is reduced. Compared with CG, the UVAG grinding wheel has better self-sharpening performance and grinding stability.

The grinding force consists of two components, the chip deformation force and friction force, and can be described by Equation (10) [31].

$$F = F_c + F_f \tag{10}$$

where F_c is the chip deformation force, and F_f is the friction force. F_c is related to the inherent characteristics of materials and the setting of processing parameters. Under the same processing parameters, the chip deformation force of CG and UVAG can be assumed to be constant. The above analysis shows that UVAG can reduce the frictional force of the grinding process, and thus, UVAG can obtain a low grinding force. As shown in Figure 6, the grinding force in CG and UVAG decreases with increasing spindle speed and increases with increasing feed rate and grinding depth. At the same time, the grain state of the grinding wheel surface before and after grinding was observed and counted, as shown in Figure 5. The number of grains pulled out tends to decrease with increasing spindle speed and increase with increasing feed rate and grinding depth. It can be seen that with the change in grinding process parameters, the wear form of the grinding wheel and the change in grinding force have a certain linear relationship

4.3. Surface Quality

From the above analysis, the wear of grains in UVAG is mainly in the form of microfracture, which increases the number of cutting edges, and the grinding wheel achieves effective self-sharpening.

Although there is also grain microfracture in CG, the grinding trajectory produced by the microfracture has no interference and produces groove-like scratches, and each groove has no crossover phenomenon, which is not conducive to reducing the *Ra* value, as shown in Figure 12a. However, the trajectory of grain movement in UVAG is sinusoidal cutting, and sinusoidal grooves are produced during grinding; the effective cutting edge of a single grain increases after the grain undergoes microfracture, and multiple sinusoidal grooves are produced during grinding.

As shown in Figure 12b, the height of the compounded sinusoidal groove decreases, and the grinding surface becomes smoother due to the mutual interference of the grinding trajectories in UVAG, resulting in a lower *Ra* value. In addition, the cutting edges produced by the fragmentation of individual grains in UVAG are close to each other, and grinding produces more interfering sinusoidal grooves with more trajectory intersections, which favors the reduction in the sinusoidal groove height and leads to a reduction in R_z. Figure 13 shows the surface profiles of the two grinding methods with the same processing parameters. The ultrasonic-assisted R_z is reduced by 45%, and the surface is flatter.
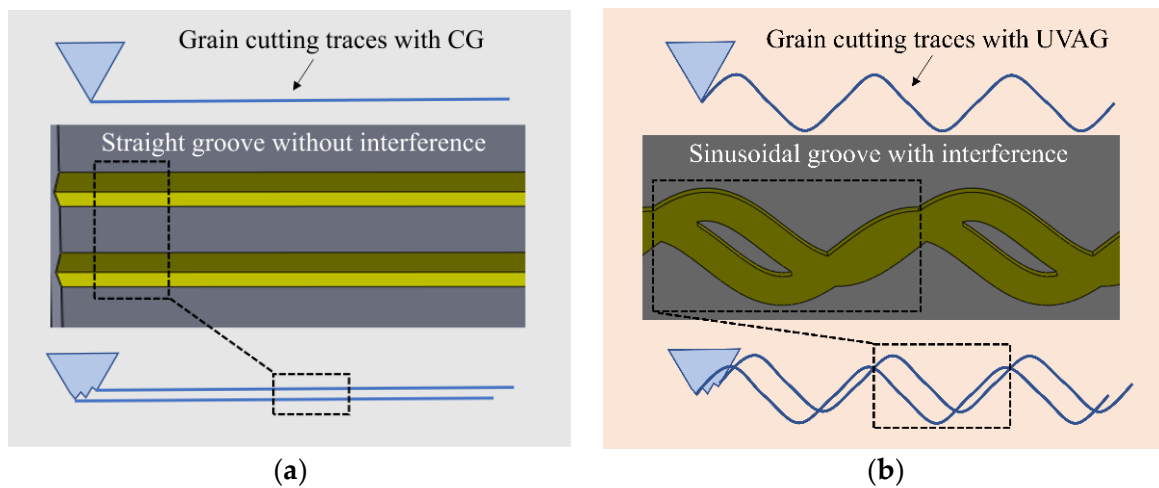
Figure 12. Microfracture trajectory of grains: (**a**) CG without crossover and (**b**) UVAG with crossover.

(**a**)
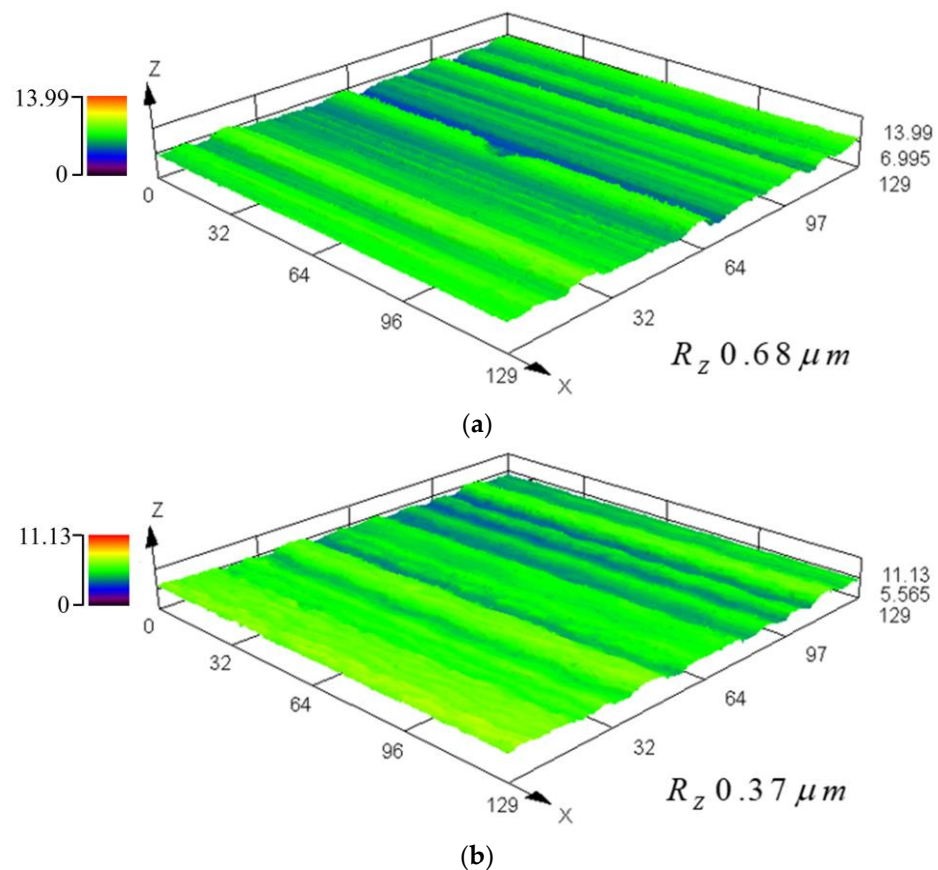

(**b**)

Figure 13. Three-dimensional grinding morphology: (**a**) CG and (**b**) UVAG.

5. Conclusions

In this work, the friction energy distribution of CG and UVAG grains in the grinding process of zirconia ceramics was studied based on the grinding trajectories of grains. The reasons for the decrease in friction energy and the microfracture of grains in UVAG were discussed. The main results are summarized as follows:

1. In UVAG, the grinding surface of the grain changes, and the generated friction energy is distributed. The friction energy of a single grinding surface is reduced, and microfracture easily occurs.

2. When the angle of the grain plunge is 90° and 150°, compared with CG, the friction energy generated by the UVAG grain grinding surface is reduced by 24% and 37%.
3. In UVAG, the microfracture of grains produces more effective cutting edges, which can obtain a better grinding surface quality. Compared with CG, Ra decreased by 12.3% and Rz decreased by 45.6%.

Data Availability Statement: Data are all contained within the article. All data are fully available without restriction.

Conflicts of Interest: The authors declare no conflict of interest.

References

1. Xiao, X.Z.; Zheng, K.; Liao, W.H.; Meng, H. Study on cutting force model in ultrasonic vibration assisted side grinding of zirconia ceramics. *Int. J. Mach. Tools Manuf.* **2016**, *104*, 58–67. [CrossRef]
2. Manicone, P.F.; Iommetti, P.R.; Raffaelli, L. An overview of zirconia ceramics: Basic properties and clinical applications. *J. Dent.* **2007**, *35*, 819–826. [CrossRef]
3. Soon, G.; Pingguan-Murphy, B.; Lai, K.W.; Akbar, S.A. Review of zirconia-based bioceramic: Surface modification and cellular response. *Ceram. Int.* **2016**, *42*, 12543–12555. [CrossRef]
4. Zhang, Y.; Lawn, B.R. Novel Zirconia Materials in Dentistry. *J. Dent. Res. Off. Publ. Int. Assoc. Dent. Res.* **2018**, *97*, 140–147. [CrossRef] [PubMed]
5. Zhang, X.H.; Kang, Z.X.; Li, S.; Shi, Z.Y.; Wen, D.D.; Jiang, J.; Zhang, Z.C. Grinding force modelling for ductile-brittle transition in laser macro-micro-structured grinding of zirconia ceramics. *Ceram. Int.* **2019**, *45*, 18487–18500. [CrossRef]
6. Ji, B.; Alrayes, A.A.; Zhao, J.; Feng, Y.Z.; Shen, Z.J. Grinding and polishing efficiency of a novel self-glazed zirconia versus the conventional dry-pressed and sintered zirconia ceramics. *Adv. Appl. Ceram.* **2018**, *118*, 46–55. [CrossRef]
7. Dai, S.; Lei, H.; Fu, J.F. Self-assembly preparation of popcorn-like colloidal silica and its application on chemical mechanical polishing of zirconia ceramic. *Ceram. Int.* **2020**, *46*, 24225–24230. [CrossRef]
8. Zhang, X.H.; Wang, Z.R.; Shi, Z.Y.; Shi, Z.J.; Jiang, R.Y.; Kang, Z.X. Improved grinding performance of zirconia ceramic using an innovative biomimetic fractal-branched grinding wheel inspired by leaf vein—ScienceDirect. *Ceram. Int.* **2020**, *46*, 22954–22963. [CrossRef]
9. Zhang, M.H.; Pang, Z.X.; Jia, Y.X.; Shan, C.W. Understanding the machining characteristic of plain weave ceramic matrix composite in ultrasonic-assisted grinding. *Ceram. Int.* **2022**, *48*, 5557–5573. [CrossRef]
10. Kwon, W.; Kim, T.; Song, K.Y. Experimental Investigation on CO_2 Laser-Assisted Micro-Grinding Characteristics of Al_2O_3. *Int. J. Precis. Eng. Manuf.* **2021**, *22*, 51–62. [CrossRef]
11. Rao, X.S.; Zhang, F.H.; Li, C.; Li, Y.J. Experimental investigation on electrical discharge diamond grinding of RB-SiC ceramics. *Int. J. Adv. Manuf. Technol.* **2018**, *94*, 2751–2762. [CrossRef]
12. Zhao, B.; Chang, B.Q.; Wang, X.B.; Bie, W.B. System design and experimental research on ultrasonic assisted elliptical vibration grinding of Nano-ZrO_2 ceramics. *Ceram. Int.* **2019**, *45*, 24865–24877. [CrossRef]
13. Kadivar, M.; Shamray, S.; Soltani, B.; Daneshi, A.; Azarhoushang, B. Laser-assisted micro-grinding of Si_3N_4. *Precis. Eng.* **2019**, *60*, 394–404. [CrossRef]
14. Ma, Z.L.; Wang, Q.H.; Dong, J.D.; Wang, Z.; Yu, T.B. Experimental investigation and numerical analysis for machinability of alumina ceramic by laser-assisted grinding. *Precis. Eng.* **2021**, *72*, 798–806. [CrossRef]
15. Kumar, M.; Satsangi, P.S. A study on machining performance of wire electric discharge grinding (WEDG) process during machining of tungsten alloy micro-tools. *Sadhana* **2021**, *46*, 1–11. [CrossRef]
16. Rao, X.S.; Zhang, F.H.; Lu, Y.J.; Luo, X.C.; Chen, F.M. Surface and subsurface damage of reaction-bonded silicon carbide induced by electrical discharge diamond grinding. *Int. J. Mach. Tools Manuf.* **2020**, *154*, 103564. [CrossRef]
17. Zhang, Q.J.; Li, J.Y.; Cai, Y.L.; Wang, H. Study on Electrical Discharge and Ultrasonic Assisted Mechanical Combined Machining of Polycrystalline Diamond. *Procedia CIRP* **2013**, *6*, 589–593.
18. Das, S.; Pandivelan, C. Grinding characteristics during ultrasonic vibration assisted grinding of alumina ceramic in selected dry and MQL conditions. *Mater. Res. Express* **2020**, *7*, 85404. [CrossRef]
19. Ding, K.; Fu, Y.C.; Su, H.H.; Gong, X.B.; Wu, K.Q. Wear of diamond grinding wheel in ultrasonic vibration-assisted grinding of silicon carbide. *Int. J. Adv. Manuf. Technol.* **2014**, *71*, 1929–1938. [CrossRef]

20. Shen, J.Y.; Wang, J.Q.; Jiang, B.; Xu, X.P. Study on wear of diamond wheel in ultrasonic vibration-assisted grinding ceramic. *Wear* **2015**, *332–333*, 788–793. [CrossRef]

21. Baraheni, M.; Amini, S. Mathematical model to predict cutting force in rotary ultrasonic assisted end grinding of Si_3N_4 considering both ductile and brittle deformation. *Meas. J. Int. Meas. Confed.* **2020**, *156*, 107586. [CrossRef]

22. Lei, X.F.; Xiang, D.H.; Peng, P.C.; Liu, G.F.; Li, B.; Zhao, B.; Gao, G.F. Establishment of dynamic grinding force model for ultrasonic-assisted single abrasive high-speed grinding. *J. Mater. Process. Technol.* **2022**, *300*, 117420. [CrossRef]

23. Liang, Z.Q.; Wang, X.B.; Wu, Y.B.; Xie, L.J.; Liu, Z.B.; Zhao, W.X. An investigation on wear mechanism of resin-bonded diamond wheel in Elliptical Ultrasonic Assisted Grinding (EUAG) of monocrystal sapphire. *J. Mater. Process. Technol.* **2012**, *212*, 868–876. [CrossRef]

24. Ding, K.; Fu, Y.C.; Su, H.H.; Xu, H.X.; Cui, F.F.; Li, Q.L. Experimental studies on matching performance of grinding and vibration parameters in ultrasonic assisted grinding of SiC ceramics. *Int. J. Adv. Manuf. Technol.* **2017**, *88*, 2527–2535. [CrossRef]

25. Zheng, K.; Li, Z.H.; Liao, W.H.; Xiao, X.Z. Friction and wear performance on ultrasonic vibration assisted grinding dental zirconia ceramics against natural tooth. *J. Braz. Soc. Mech. Sci. Eng.* **2017**, *39*, 833–843. [CrossRef]

26. Zou, L.; Huang, Y.; Zhou, M.; Duan, L. Investigation on diamond tool wear in ultrasonic vibration-assisted turning die steels. *Mater. Manuf. Process.* **2006**, *32*, 1505–1511. [CrossRef]

27. Tsai, C.; Tseng, C. The effect of friction reduction in the presence of in-plane vibrations. *Arch. Appl. Mech.* **2006**, *75*, 164–176. [CrossRef]

28. Wu, B.F.; Zhao, B.; Ding, W.F.; Su, H.H. Investigation of the wear characteristics of microcrystal alumina abrasive wheels during the ultrasonic vibration-assisted grinding of PTMCs. *Wear* **2021**, *477*, 203844. [CrossRef]

29. Agarwal, S.; Venkateswara, R.P. Predictive modeling of undeformed chip thickness in ceramic grinding. *Int. J. Mach. Tools Manuf.* **2012**, *56*, 59–68. [CrossRef]

30. Yang, Z.C.; Zhu, L.D.; Lin, B.; Zhang, G.X.; Ni, C.B.; Sui, T.Y. The grinding force modeling and experimental study of ZrO_2 ceramic materials in ultrasonic vibration assisted grinding. *Ceram. Int.* **2019**, *45*, 8873–8889. [CrossRef]

31. Ren, J.X.; Huang, D.A. *Grinding Principle*, 1st ed.; Publishing House of Electronics Industry: Beijing, China, 2011; pp. 41–61.